Available online at www.sciencedirect.com

SciVerse ScienceDirect

Ceramics International 39 (2013) S129–S133

CERAMICS INTERNATIONAL

www.elsevier.com/locate/ceramint

The effects of aliovalent cations doping on electric-field-induced strain and microstructures of $(Bi_{0.5}Na_{0.5})_{0.94}Ba_{0.06}TiO_3$ lead-free piezoceramics

Pin-Yi Chen[a], Chen-Chia Chou[b,*], Cheng Nan Chen[b], Cheng-Sao Chen[c], Haydn Chen[d]

[a]*Department of Mechanical Engineering, Ming-Chi University of Technology, New Taipei City 243, Taiwan*
[b]*Department of Mechanical Engineering, National Taiwan University of Science and Technology, Taipei City 106, Taiwan*
[c]*Department of Mechanical Engineering, Hwa-Hsia Institute of Technology, New Taipei City, Taipei 235, Taiwan*
[d]*Department of Physics, Tunghai University, Taichung City 407, Taiwan*

Available online 16 October 2012

Abstract

Effects of Al and Nb doped $(Bi_{0.5}Na_{0.5})_{0.94}Ba_{0.06}TiO_3$(abbreviated as BNB6T) ceramics on dielectric, ferroelectric, and strain properties were investigated. The results indicated that the d_{33}^* value is significantly higher in pure BNB6T ceramics than in Nb doped BNB6T and Al doped BNB6T ceramics, and that *S–E* curve for the Al doped BNB6T ceramics displayed a typical W-shaped butterfly curve, but pure BNB6T and Nb doped BNB6T ceramics display a V-shaped curve. The *P–E* loops for pure BNB6T and Nb doped BNB6T ceramics were similar to soft PZT ceramics with slim profiles. According to the results of microstructures analysis, significant strain may originate from the development of the optimum compound domains coexistence (the mixture of microdomain and nanodomain), which provide large saturation polarization and low-energy barrier dipole switching under an applied electric field. All these would provide a new concept for lead-free ceramics to realize high strain response for practical applications in actuator or other piezoelectric devices.

Keywords: B. Microstructure-final; C. Ferroelectric properties; D. Perovskites

1. Introduction

Electric field induced strain is one of the most important parameters for electromechanical actuators. Lead zirconate titanate (PZT) ceramics are widely used in electromechanical actuators because of their excellent piezoelectric properties. However, in recent years, nontoxic piezoceramics have been studied extensively since the RoHS/WEEE regulations restricting lead-containing piezoceramics were introduced. Recently, BNT-based materials are expected to be a superior lead-free candidate material because they exhibit a field-induced giant strain that is suitable for many large-scale applications, such as piezo-buzzer, piezo energy harvesting, piezo-injectors, and ink jet printers.

The $(Bi_{0.5}Na_{0.5})_{1-x}Ba_xTO_3$ system (abbreviated as BNBxT) has attracted considerable attention worldwide since the discovery of an MPB in the system in 1991 [1], where rhombohedral and a tetragonal symmetry coexist. Consequently, research interest has grown considerably regarding the BNBxT because the MPB compositions caused significant enhancements in the dielectric, ferroelectric, and piezoelectric properties. Recently, large strains have been reported for BNT-based solid solutions [2–5]. Zhang et al. [3,4] have suggested that large strains are attributed to the structural phase transition between the antiferroelectric and ferroelectric, and Teranishi et al. [5] have suggested that the large strains are caused by 90°domain switching in the tetragonal phase by the X-ray diffraction pattern under a high electric field. Hiruma et al. proposed that the large strains are caused by the field-induced phase transition and the non-180° domain switching of the field-induced rhombohedral phase [2]. In the

*Corresponding author. Tel.: +886 2 27376493; fax: +886 2 27376460.
E-mail address: ccchou@mail.ntust.edu.tw (C.-C. Chou).

0272-8842/$ - see front matter © 2012 Elsevier Ltd and Techna Group S.r.l. All rights reserved.
http://dx.doi.org/10.1016/j.ceramint.2012.10.048

recent 3–4 years, studied on electrical field induced large strain in lead-free BNT-based materials have particularly focused on identifying the phase transition, which affects electrical properties and strain behaviors. Therefore, the correlations among the microstructures, strain, and electrical properties are important to develop new lead-free piezoelectric materials. On the other hand, doping also affects crystal structure and phase transition behaviors. Nevertheless, combination studies of the acceptor and donor doping effects on the new lead-free system are few reported. In this study, Al and Nb modified BNT–BT solid solutions were developed and their microstructures, electrical properties, and strain behaviors were studied.

2. Experimental

A conventional mixed-oxide solid state reaction technique was used to fabricate the lead-free $(Bi_{0.5}Na_{0.5})_{0.094}Ba_{0.06}(T_{1-x}B_x)O_3$ ($B=Al^{3+}$, Nb^{5+}) ceramics with $x=0$, 0.01, 0.02, and 0.03. Commercially available Bi_2O_3, Na_2CO_3, $BaCO_3$, TiO_2, Al_2O_3,and Nb_2O_5 ceramics with purities higher than 99.9% were mixed in ethanol and milled with zirconia balls for 24 h. Subsequently, the mixed powders were calcined at 850 °C for 2 h, and were sintered at 1150 °C for 2 h in air atmosphere. The crystal structure and morphology were observed using X-ray diffraction (XRD, D-2 phaser, Bruker AXS) and transmission electron microscope (FEG–TEM; Tecnai G2 F20). For the electrical measurements, the samples were plated with a silver paste and fired at 750 °C for 30 min. The *P–E* and *S–E* hysteresis loops were measured using a Radiant Precision Workstation 2000 system connected to a MTI 2000 displacement meter. The dielectric constant and loss tangent were measured using an HP4194 gain-phase analyzer at a frequency within 100 Hz-1 MHz and the temperature range from 25 to 400 °C.

3. Results and discussions

The densities of the all sintered specimens were measured using the Archimedes method. The density range of the measured specimens is 5.8–6.0 g/cm^3 and the relative densities of all specimens were above 95% compared to their theoretical density. Because the amount of doping was appropriate, no extra phases were found below 3 mol% doping compositions.

Fig. 1 shows electric field induced strain behavior (*S–E* curve) for the pure BNB6T, Al doped BNB6T, and Nb doped BNB6T ceramics, which had bipolar strains of 0.109%, 0.149%, and 0.245%, respectively. Following calculation, the S_{max}/E_{max} (d^*_{33}) values were 200 pm/V, 275 pm/V, and 475 pm/V. The strain and d^*_{33} of the pure BNB6T are higher than those of the Nb doped BNB6T and Al doped BNB6T. In addition, the value of d^*_{33} in the pure BNB6T was similar to that in soft PZT (400–590 pm/V). Further comparison with the profiles shown in Fig. 1 showed that the pure BNB6T and Nb doped BNB6T display a

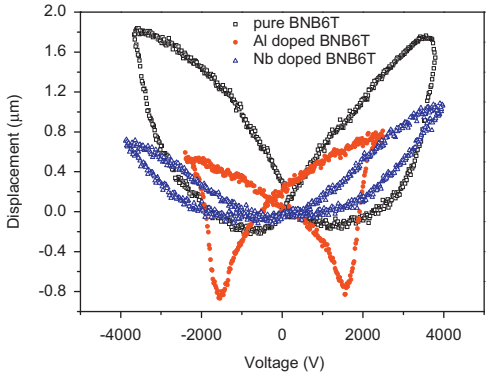

Fig. 1. Bipolar field-induced strains with pure BNB6T ceramics, Al doped 2 mol% BNB6T ceramics, and Nb doped 2 mol% BNB6T ceramics measured at 4 Hz.

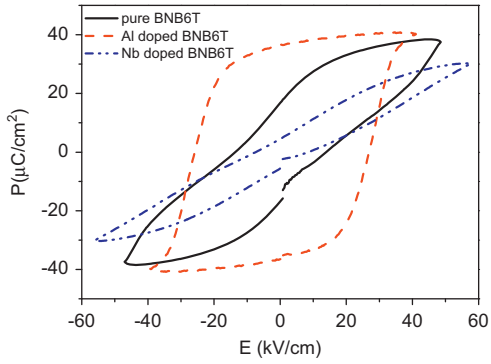

Fig. 2. Polarization hysteresis loops of pure BNB6T ceramics, 2 mol% Al doped BNB6T ceramics, and 2 mol% Nb doped BNB6T ceramics.

V-shaped curve, but the Al doped BNB6T displayed typical ferroelectric features with a W-type butterfly curve. Both profiles were substantially different, and the results may imply that there are different mechanisms for electric field induced strain in Al-doped and Nb-doped BNBT ceramics. This issue is discussed below.

Fig. 2 shows the *P–E* hysteresis loops for pure BNB6T, Al doped, and Nb doped BNB6T ceramics at room temperature. For these *P–E* loops, both the pure BNB6T and the Nb doped BNB6T exhibited slim profiles, although the profile of the Nb doped BNB6T is slimmer than that of the pure BNB6T. However, the *P–E* loop of Al doped BNB6T ceramics was not similar to those of the pure BNB6T and Nb doped BNB6T and it became a typical ferroelectric hysteresis loop. The results were consistent with the characteristic of *S–E* curves. On the other hand, it was observed that the dielectric losses increased drastically for the Al doped BNB6T ceramics compared to the pure BNB6T and Nb doped BNB6T ceramics. The dielectric losses of the Al doped specimen increased as the temperature increased, which may imply the existence of high ionic conductivity. Replacing the Ti^{4+} ions of B-site with Al^{3+} ions produced oxygen vacancies that were determined by charge balance. Therefore, the higher dielectric loss in the Al doped BNB6T ceramics could be attributed to increased

oxygen vacancies. It has been previously demonstrated that oxygen vacancies are one of the main causes of reduction the domain-wall motion [6,7]. A larger amount of oxygen vacancies reduced the switching ability of polarization, making it more difficult to switch polarization vectors under the applied electric field, resulting in the increase of the coercive field. The result is more consistent with the larger coercive field in the Al doped BNB6T than those in the pure BNB6T and Nb doped BNB6T ceramics as shown in Fig. 2.

Fig. 3(a) shows the XRD patterns of the pure BNB6T, Al doped, and Nb doped specimens. The patterns of all the specimens revealed a primarily perovskite structure. The differences among these XRD patterns can be observed around the 2θ of 46°–48° as shown in Fig. 3(b). The pure BNB6T ceramics split into two peaks, but the Al doped BNB6T ceramics tended to have a single peak. Meanwhile, the Nb doped BNB6T ceramics still keep the splitting of two peaks but appeared to tend toward a single peak tendency.

These results indicate that a small amount of doping affect phase transition in BNB6T ceramics. Jo et al. [8] used neutron diffraction to identify the weak changes in crystal structure and proposed the coexistence of tetragonal ($a^0a^0c^+$) and rhombohedral ($a^-a^-a^-$) distortion structures in BNB6T ceramics. Therefore, the BNB6T ceramics are a two-phase coexistence material of rhombohedral and tetragonal phases. However, the Al doped specimens tended toward a single peak, which may indicate that they favor a rhombohedral phase structure transition. The Nb doped composition still maintains to split into two peaks, implying two-phase coexistence, although the profiles from the x-ray showed a tendency toward a rhombohedral phase structure.

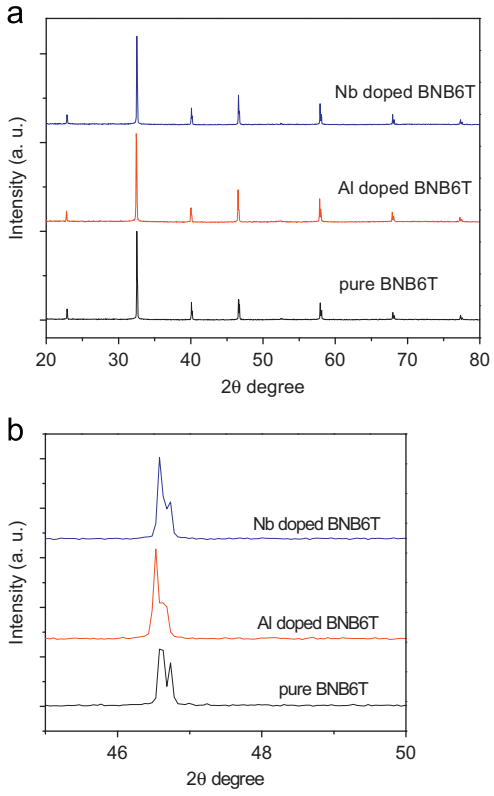

Fig. 3. (a) X-ray diffraction patterns of the pure BNB6T, 2 mol% Al-doped, and 2 mol% Nb-doped BNB6T ceramics and (b) reflections around 2θ of 45–50°.

To better understand the microstructures, TEM observations were carried out on the specimens. The pure BNB6T ceramics revealed some core-shell-like images, shown in Fig. 4(a). The core region exhibited features of sub-micron complex domains, and the shell region displayed a tweed-like image, although there were no evident domain features. The shell image was observed along the (001) zone axis using high resolution electron microscopy (HRTEM) and exhibited several short-range order in atomic arrangement as shown in Fig. 4(b). These short-range order atoms represent nano-scale domains and nano-polar regions (PNRs) structures are probably prevalent in BNB6T ceramics. Ma et al. [9] discovered the core-shell structure and proposed that the core belongs to rhombohedral phase (space group of *R*3*c*), whereas the shell belongs to tetragonal phase (space group of *P*4*bm*). The further electron diffraction patterns (EDP) analysis discovered the presence of the super lattice diffraction spots at several specific zone axes that originate from octahedral tilting. The selected area electron diffraction (SAED) was performed on pure BNB6T ceramics and the core structures revealed the presence of strong 1/2 (131) superlattice diffraction spots along the (013) zone axis as shown in Fig. 4(c). However, the shell structures revealed the presence of strong 1/2 (031) and 1/2 (131) superlattice diffraction spots along the (013) zone axis as shown in Fig. 4(d). According to previous studies [10,11], the rhombohedral distortion structure with an *R*3*c* space group is characterized by the presence of 1/2 (too) super lattice diffraction spots, whereas the tetragonal distortion structure with a *P*4*bm* space group is accompanied by the 1/2 (oboe) super lattice spots (o stands for odd and e stands for even miller indices). Therefore, the core structure in the pure BNB6T ceramics indicates the presence of a rhombohedral phase and shell structure indicates the coexistence of the rhombohedral and tetragonal phases. Some streaking super lattice spots occurred in tetragonal phase with tweed-like image. Therefore, the tetragonal phase may possess a platelet feature that is approximately a nanometer thick. TEM analysis showed that the coexistence of rhombohedral and tetragonal phases in the pure BNB6T ceramics, which was consistent with the X-ray analysis. On the other hand, the Al doped BNB6T ceramics exhibited evidence for the ferroelectric domain, as shown in Fig. 4(e), and dispersed at the local area within the specimen. However, the microstructures of the pure BNB6T ceramics were different and it might be attributed to the combinations of the microdomains or nanodomains that were caused by interactions with oxygen vacancies, which might induce the macroscopic ferroelectric domain. The SAED in the Al doped BNB6T ceramics indicated the presence of strong 1/2 (111) superlattice diffraction spots

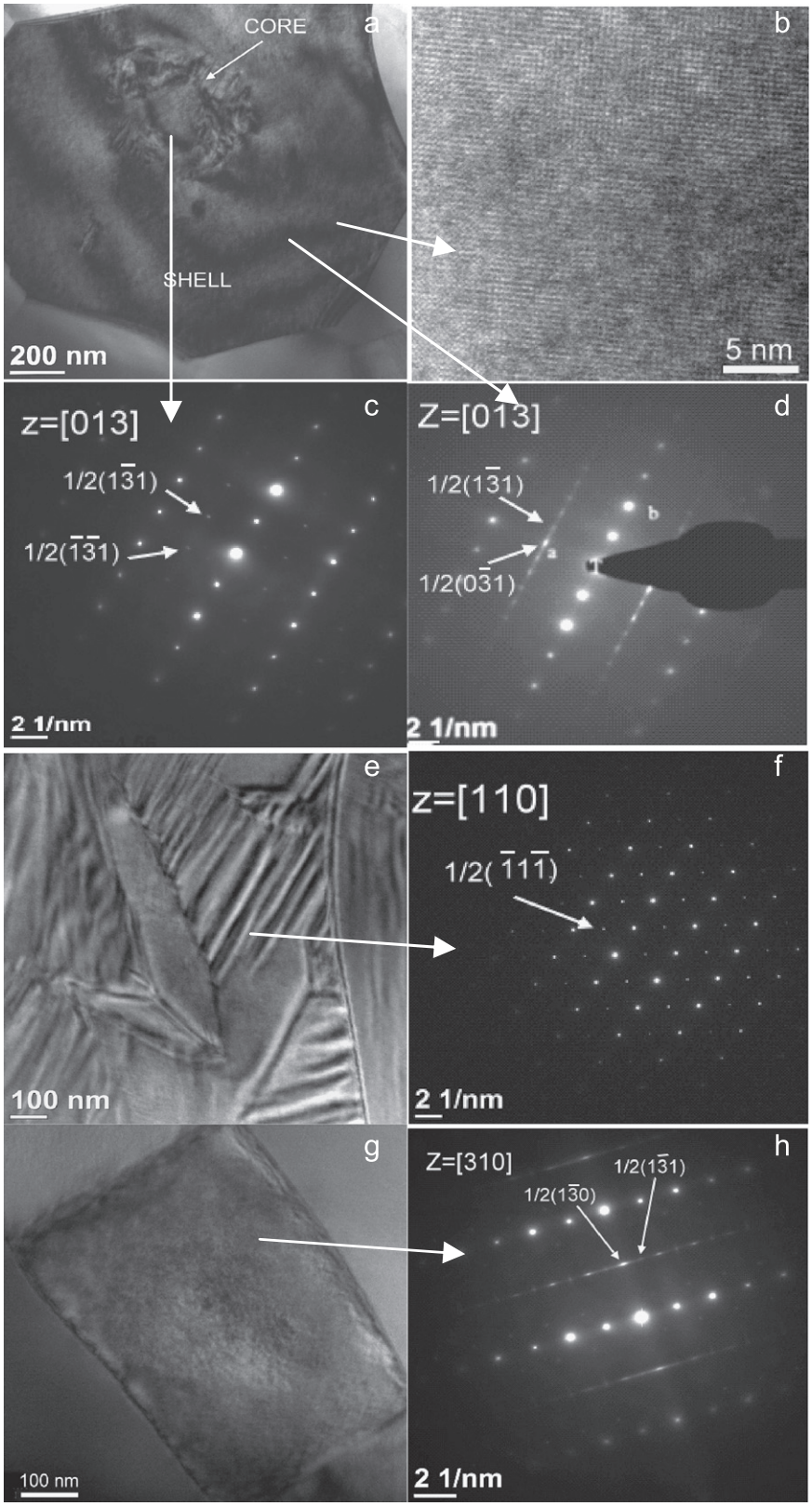

Fig. 4. (a) TEM bright field image in a representative grain for the composition of the pure BNB6T ceramics with core-shell structures; (b) high resolution electron microscopy image viewed along the (001) zone axis (note the appearance of several nano-scale domains); (c) SAED of a core along the (110) zone axis; (d) SAED of a shell along the (111) zone axis; (e) TEM bright field image of the Al doped BNB6T ceramics; (f) SAED of the Al doped BNB6T along the (011) zone axis; (g) TEM bright field image of the Nb doped BNB6T ceramics; (h) SAED of the Nb doped BNB6T along the (310) zone axis.

along the (110) zone axis, as shown in Fig. 4(f). These patterns show the rhombohedral structure of octahedral tilting and the domain image reveals a non-90° domain. Therefore, the Al doped BNB6T ceramics may possess substantially more rhombohedral structures than the pure BNB6T ceramics. These results are in agreement with the X-ray analysis. Finally, the Nb doped BNB6T ceramics revealed several tweed-like images, as shown in Fig. 4(g). The image with the corresponding SAED showed the presence of 1/2 (131) and streaking 1/2 (130) superlattice diffraction spots along the (310) zone axis, as shown in Fig. 4(h), and the results indicated the coexistence of rhombohedral and tetragonal structures.

4. Conclusions

According to the analysis in the study, the pure BNB6T ceramics displayed the largest strain. The large strain mechanism may be related to the ratio of two phases. The pure BNB6T, Al doped, and Nb doped BNB6T ceramics are composed of the rhombohedral phase with microdomain features and the tetragonal phases with nanodomain features, although the ratios of two phases differ among the three materials. The BNB6T ceramics are the solid solution of BNT and BT ceramics. The pure BNT ceramics indicate a rhombohedral structure (*R*3*c* space group) at room temperature and it displays strong ferroelectric features with high saturation polarization (P_s) and remanent polarization (P_r). In this study, the tetragonal phase (space group is *P*4*bm*) of the pure BNB6T, Al doped, and Nb doped BNB6T ceramics reveals a nanodomain with a low energy barrier feature of dipole switching. Because electric field-induced large strain needs to possess high saturation polarization and the high dipole switching ability in the materials, the rhombohedral phase provides high saturation polarization and the tetragonal phase contributes the low energy barrier of dipole switching in the three materials. The pure BNB6T ceramics display the largest electric field-induced strain. It might be attributed to the optimum fraction coexistence of rhombohedral and tetragonal phases. The results in the study can lead to improvement in current understanding of high-strain phenomena in similar materials.

Acknowledgments

This project is supported by National Science of Council of Taiwan under Project nos. 97-2923-M-029-001-MY3, 99-2221-E-011-043-MY2, and 100-2221-E-131-014.

References

[1] T. Takenaka, K.-I. Maruyama, K. Sakata, $(Bi_{1/2}Na_{1/2})TiO_3$–$BaTiO_3$ system for lead-free piezoelectric ceramics, Japanese Journal of Applied Physics 30 (Part 1) (1991) 2236–2239.

[2] Y. Hiruma, Y. Imai, Y. Watanabe, T. Takenaka, Large electrostrain near the phase transition temperature of $(Bi_{0.5}Na_{0.5})TiO_3$–$SrTiO_3$ ferroelectric ceramics, Applied Physics Letters 92 (2008) 262904.

[3] S.T. Zhang, A.B. Kounga, E. Aulbach, J. Rodel, Giant strain in lead-free piezoceramics$Bi_{0.5}Na_{0.5}TiO_3$–$BaTiO_3$–$K_{0.5}Na_{0.5}NbO_3$ system, Applied Physics Letters 91 (2007) 112906.

[4] S.T. Zhang, A.B. Kounga, E. Aulbach, W. Jo, T. Granzow, H. Ehrenberg, J. Rödel, Lead-free piezoceramics with giant strain in the system $Bi_{0.5}Na_{0.5}TiO_3$–$BaTiO_3$–$K_{0.5}Na_{0.5}NbO_3$. II temperature dependent properties, Journal of Applied Physics 103 (2008) 034108.

[5] S. Teranishi, M. Suzuki, Y. Noguchi, M. Miyayama, C. Moriyoshi, Y. Kuroiwa, K. Tawa, S. Mori, Giant strain in lead-free $(Bi_{0.5}Na_{0.5})$-TiO_3-based single crystals, Applied Physics Letters 92 (2008) 182905.

[6] S.E. Park, S.J. Chung, Ferroicphase transitions in $(Na_{1/2}Bi_{1/2})TiO_3$ crystals, Journal of the American Ceramic Society 79 (1996) 1290–1296.

[7] U. Robels, L. Schneider-Stomann, G. Arlt, Domain wall trapping as a result of internal bias fields, Ferroelectrics 133 (1992) 223–228.

[8] W. Jo, J.E. Daniels, J.L. Jones, X. Tan, P.A. Thomas, Evolving morphotropic phase boundary in lead-free $(Bi_{1/2}Na_{1/2})TiO_3$–$BaTiO_3$ piezoceramics, Journal of Applied Physics 109 (2011) 014110.

[9] C. Ma, X. Tan, E. Dul'kin, M. Roth, Domain structure-dielectric property relationship in lead-free $(1-x)(Bi_{1/2}Na_{1/2})TiO_3$–$xBaTiO_3$ ceramics, Journal of Applied Physics 108 (2010) 104105.

[10] D.I. Woodward, I.M. Reaney, Electron diffraction of tilted perovskites, Acta Crystallographica Section B: Structural Science 61 (2005) 387–399.

[11] A.M. Glazer, Crystal physics, simple ways of determining perovskite structures, Acta Crystallographica Section A. Crystal Physics, Diffraction, Theoretical and General Crystallography 31 (1975) 756–762.